Adenomatous Polyposis Coli (APC) Protein Moves along Microtubules and Concentrates at Their Growing Ends in Epithelial Cells✪

Yuko Mimori-Kiyosue,* Nobuyuki Shiina,* and Shoichiro Tsukita*‡

*Tsukita Cell Axis Project, Exploratory Research for Advanced Technology, Japan Science and Technology Corporation, Kyoto Research Park, Shimogyo-ku, Kyoto 600-8813, Japan; and ‡Department of Cell Biology, Faculty of Medicine, Kyoto University, Sakyo-ku, Kyoto 606-8315, Japan

Abstract. Adenomatous polyposis coli (APC) tumor suppressor protein has been shown to be localized near the distal ends of microtubules (MTs) at the edges of migrating cells. We expressed green fluorescent protein (GFP)-fusion proteins with full-length and deletion mutants of *Xenopus* APC in *Xenopus* epithelial cells, and observed their dynamic behavior in live cells. During cell spreading and wound healing, GFP-tagged full-length APC was concentrated as granules at the tip regions of cellular extensions. At higher magnification, APC appeared to move along MTs and concentrate as granules at the growing plus ends. When MTs began to shorten, the APC granules dropped off from the MT ends. Immunoelectron microscopy revealed that fuzzy structures surrounding MTs were the ultrastructural counterparts for these GFP signals. The COOH-terminal region of APC was targeted to the growing MT ends without forming granular aggregates, and abruptly disappeared when MTs began to shorten. The APC lacking the COOH-terminal region formed granular aggregates that moved along MTs toward their plus ends in an ATP-dependent manner. These findings indicated that APC is a unique MT-associated protein that moves along selected MTs and concentrates at their growing plus ends through their multiple functional domains.

Key words: adenomatous polyposis coli • green fluorescent protein • microtubules • microtubule-associated proteins • epithelial cells

Introduction

Microtubules (MTs)[1] are polarized tubular structures which are produced by linear polymerization of α/β-tubulin heterodimers, with the plus end favored for assembly over the minus end (Binder et al., 1975; Bergen and Borisy, 1980). It is now widely accepted that MTs are involved in cellular morphogenesis in various ways. As motor molecules such as dyneins and kinesins utilize the polarity of MTs to translocate toward their plus and minus ends, respectively, MTs provide tracks or scaffolds for the directional vesicle transport as well as organelle positioning (Cole and Lippincott-Schwartz, 1995; Goodson et al., 1997). Furthermore, MTs themselves are structurally very dynamic both in vitro and in vivo.

In migrating cells, MTs are generally polarized along the axis of cell movement with their plus ends facing the leading edge (Gotlieb et al., 1981). Although the role of MTs in cell migration still remains unclear, MTs themselves and their dynamics have been shown to be required for fibroblasts, epithelial cells, neuronal growth cones, etc., to move directionally with concomitant dynamic remodeling of cellular structures (Vasiliev, 1991; Liao et al., 1995; Tanaka et al., 1995). In this connection, the dynamic behavior of the plus ends of MTs at the leading edge has been examined extensively (Cassimeris et al., 1988; Sammak and Borisy, 1988; Schulze and Kirschner, 1988). The plus ends of MTs are known to display dynamic instability in vitro as well as in vivo (Mitchison and Kirschner, 1984), and the parameters for dynamic instability are modulated by a number of MT accessory proteins in a cell-type specific manner (Shelden and Wadsworth, 1993; Desai and Mitchison, 1997). Also, in the leading edge some selected microtubules appeared to be differentially regulated in terms of their dynamic instability at plus ends (Waterman-Storer and Salmon, 1997), which would be important for dynamic morphogenesis at the leading edge of migrating cells (Kirschner and Mitchison, 1986). Therefore, further stud-

✪The online version of this article contains supplemental material.

Address correspondence to Shoichiro Tsukita, Department of Cell Biology, Kyoto University Faculty of Medicine, Konoe-Yoshida, Sakyo-ku, Kyoto 606-8315, Japan. Tel.: 81 75-753-4372. Fax: 81 75-753-4660. E-mail: htsukita@mfour.med.kyoto-u.ac.jp

[1]*Abbreviations used in this paper:* aa, amino acids; AMP-PNP, 5′-adenylylimidodiphosphate; APC, adenomatous polyposis coli; GFP, green fluorescent protein; MAP, microtubule-associated protein; MT, microtubule; pAb, polyclonal antibody.

ies of the molecular mechanism behind the regulation of dynamic instability of MTs in localized areas such as the leading edge will lead to a better understanding of how MTs are involved not only in cell migration but also in polarized cellular morphogenesis.

From these viewpoints, the subcellular localization of adenomatous polyposis coli (APC) protein in cultured MDCK epithelial cells is intriguing (Näthke et al., 1996; Barth et al., 1997b; Pollack et al., 1997). In these cells, endogenous APC was localized in clusters of puncta near the ends of MTs at peripheral membrane sites of migrating edges, and this localization required intact MTs. In addition to these pioneering works, an intimate relationship between APC protein and MTs (or MT-dependent cell migration) has been suggested from both in vitro and in vivo observations. Biochemical analyses indicated that APC protein directly bound to MTs, and that the COOH-terminal region of APC protein promoted the nucleation of tubulin polymerization in vitro (Munemitsu et al., 1994; Deka et al., 1998). Furthermore, APC proteins overexpressed in culture cells decorated the entire length of MTs (Munemitsu et al., 1994; Smith et al., 1994). In the intestine, truncation of the COOH-terminal region of APC protein caused accumulation of enterocytes near the crypt-villus transition due to a defect in cell migration (Polakis, 1995), and forced expression of wild-type APC protein resulted in disordered cell migration (Wong et al., 1996). To date, various types of MT-associated proteins have been identified and characterized (for review see Cassimeris, 1999), but APC protein appeared to be unique in its MT-associated localization only in specialized areas of cells, which would be important for cellular morphogenesis.

The APC gene is mutated during the progression of sporadic colorectal tumors as well as in patients with familial adenomatous polyposis (for reviews see Nakamura, 1993; Kinzler and Vogelstein, 1996). APC protein is involved in regulation of the stability of β-catenin, and mutations in the APC gene result in carcinogenesis by stabilizing β-catenin followed by activation of the Wnt signaling pathway (Munemitsu et al., 1995; Morin et al., 1997). The APC gene encodes a 310-kD cytoplasmic protein which has multiple putative functional domains (see Fig. 1; for review see Polakis, 1997). The NH_2-terminal region contains an α-helix domain that forms a parallel coiled-coil dimer (Joslyn et al., 1993), which is followed by seven armadillo repeats. This region has been reported to bind to a protein phosphatase 2A regulatory subunit, B56 (Seeling et al., 1999). The middle part of APC protein containing 15–amino acid repeats and distinct 20–amino acid repeats directly interacts with β- or γ-catenin (Rubinfeld et al., 1993; Su et al., 1993b; Hulsken et al., 1994). This part of the molecule also binds to axin/conductin and glycogen synthase kinase-3β (GSK-3β), major components of the Wnt signaling pathway (Rubinfeld et al., 1996; Ikeda et al., 1998). The COOH-terminal region of APC protein was reported to associate with MTs, MT-binding proteins of the EB/RP family (Su et al., 1995; Renner et al., 1997; Juwana et al., 1999), cyclin-dependent kinase $p34^{cdc2}$ (Trzepacz et al., 1997), and a homologue of the *Drosophila* discs large (dlg) tumor suppressor protein (Matsumine et al., 1996).

In the present study, to further clarify the relationship between APC protein and MTs, we examined the dynamic behavior of APC protein in live cells: we constructed a green fluorescent protein (GFP) fusion protein with *Xenopus* APC protein, and introduced it into cultured *Xenopus* A6 epithelial cells. Furthermore, we constructed GFP fusion proteins with deletion mutants of APC protein, and compared them with full-length APC protein in terms of their behavior in live cells. These analyses uncovered peculiar interactions between APC protein and MTs. The results of this study will allow us to consider certain unknown function for the APC gene product.

Materials and Methods

Antibodies and Cells

Rabbit anti-GFP pAb (Clontech or MBL), rabbit anti-APC pAb specific for COOH-terminal 20 amino acids of human APC (APC(C-20); Santa Cruz Biotechnology, Inc.), mouse anti-APC mAb specific for NH_2-terminal 35 amino acids of human APC (APC(Ab-1); Oncogene), and mouse anti–α-tubulin mAb (DM1A; Sigma) were purchased from the sources shown. The *Xenopus* kidney epithelial cell line A6 was grown at 23°C without CO_2 atmosphere in 50% Leivobitz's L-15 medium (GIBCO BRL) supplemented with 10% fetal bovine serum and antibiotics (100 U/ml penicillin and 0.2 mg/ml kanamycin).

Plasmid Construction and Transfection

The expression vector (pQBI25) for the bright red-shifted GFP variant was purchased from Quantumn Biotechnologies, Inc. This vector was used to express recombinant proteins with a GFP tag at their COOH termini. Another expression vector (pGFP-C(NheI)) to express recombinant proteins with a GFP tag at their NH_2 termini was produced by modifying pQBI25. In this recombinant protein, two glycine residues were inserted between GFP and the rest of the fusion protein as a flexible spacer.

The *Xenopus* APC cDNA was cloned from a *Xenopus* oocyte cDNA library (Uni-ZAP XR cDNA library; Stratagene) by PCR using gene-specific primers with a 5′ NheI site. The PCR product was subcloned into pGEM-T Easy vector (Promega), and the construct was verified by sequencing. As summarized in Fig. 1, the following expression vectors for GFP-tagged full-length or deletion mutants of APC were constructed: pGFP-C(NheI)/APC(1-8490) for GFP-fAPC; pQBI25/APC(1-8487) for fAPC-GFP; pQBI25/APC(1-6474) for ΔcAPC-GFP; pGFP-C(NheI)/APC(6475-8490) for GFP-cAPC. To construct the expression vector for fAPC-mGFP, the GFP coding sequence was inserted into the SpeI site (nucleotide 6475) of APC cDNA.

Lipofectin (GIBCO BRL) was used for transfection of cDNAs, according to the manufacturer's protocol. Drug-resistant clones were selected in the presence of 0.6 or 0.75 mg/ml genetisin (GIBCO BRL or Calbiochem) and screened by detecting GFP signals with fluorescent microscope.

Quantification of Expression Levels of Endogenous and Exogenous APC

Expression levels of GFP-tagged full-length APC were analyzed by SDS-PAGE followed by immunoblotting. To separate the band of endogenous APC from that of GFP-tagged APC, 50 μl of Triton X-100 lysates of 1×10^7 transfectants (three clones expressing fAPC-GFP and three clones expressing fAPC-mGFP; see Fig. 2) were incubated with 1,000 U of λ-protein phosphatase (New England Biolabs Inc.) at 30°C for 30 min. The sample buffer containing 6 M urea was then added, and the samples containing lysates of 1×10^6 cells were separated by SDS-PAGE (2–8 M Urea, 3–5% acrylamide gradient gels), and electrophoretically transferred to PVDF membranes, which were incubated with anti-GFP pAb (1:1,000) or APC(Ab-1) mAb (1:100). The antibodies were detected with a blotting detection kit (Amersham).

For quantification of expression levels of endogenous and exogenous APC, we first expressed a NH_2 terminal portion (amino acids [aa] 1–284) of APC fused with GST at its COOH terminus in *E. coli*, and purified it. The amount of this purified GST fusion protein was determined densitometrically by comparing the intensity of its band after Coomassie brilliant blue staining with those of various amounts of BSA. We then compared

the intensity of immunoblotted endogenous APC and exogenous GFP-tagged APC in λ-protein phosphatase-treated cell lysates with those of immunoblotted bands of various amounts of purified APC(1-284)-GST. These bands were digitized by scanning with ScanJet IIcx (Hewlett Packard) and processed using Adobe Photoshop software. The intensity of the band was measured by densitometry using the NIH image software.

Immunofluorescence Staining

Cells (1–2 × 10^5 cells/cm^2) were cultured on coverslips for 24–48 h, washed with 70% Dulbecco's PBS(+) and fixed with 3.7% formaldehyde in the same PBS for 30–60 min. After washing with Dulbecco's PBS(−), cells were permeabilized with 0.1% Triton X-100 for 5 min, followed by incubation with 10% FBS. Samples were then incubated with the following primary antibodies for 1 h; anti-APC pAb, C-20 (×1,000) and anti–α-tubulin mAb, DM1A (×200). After washing several times, cells were labeled with secondary antibodies for 1 h. Fluorescein-conjugated sheep anti-mouse Ig antibody (Amersham), rhodamine-conjugated donkey anti–rabbit IgG antibody (Chemicon), and Texas red–conjugated sheep anti-mouse Ig antibody (Amersham) were used as secondary antibodies. Samples were then washed several times and mounted in Mowiol (Calbiochem). For visualization of plasma membranes, live cells were stained using a PKH26 red fluorescent cell linker kit (Sigma) according to the manufacturer's protocol.

Fluorescence Microscopy and Image Analysis

To observe live cells, cells were cultured on glass-bottomed dishes with No.1S cover glasses (Matsunami) in culture medium without phenol red at 23–25°C. Cells were cultured at low density (1–2 × 10^5 cells/cm^2) except for wound healing experiments. For wounding, cells cultured on glass-bottomed dishes at high density were wounded by scraping with a needle.

Images of fixed cells were acquired with an MRC-1024 laser confocal microscope (BioRad) or DeltaVision optical sectioning microscope (Version 2.00 or 2.10; Applied Precision, Inc.), equipped with Zeiss Axioplan2 (Plan Apochromat 63×/1.40 NA oil immersion objective) or Olympus IX70 (PlanApo 60×/1.40 NA or PlanApo 100×/1.40 NA oil immersion objective) microscope, respectively. Images from live cells were collected with a DeltaVision through a cooled CCD camera (Quantix-LC, Photometrics) with appropriate exposure time and time intervals. Fluorescence signals were visualized using appropriate ND filters, quad beamsplitter, and either of the following excitation and emission filters (Chroma): for GFP, 490/20 nm and 525/50 nm; for FITC, 490/20 nm and 528/38 nm; for rhodamine and PKH26, 555/28 nm and 617/50 nm, respectively.

Pixel positions, distances, and intensity on digital images were measured using the analysis function of DeltaVision. Images used for quantitative analyses were acquired with ×100 objective and effective pixel size was 0.067 × 0.067 μm. To quantify fluorescence intensities, mean background fluorescence obtained from an area of 11 × 25 pixels close to the targeted area was subtracted from mean intensity of the targeted area. In Fig. 7 d, the background-subtracted fluorescence intensities were obtained from 3 × 3 pixels at MT end (F1) and 2 × 5 pixels along the MT at 3 μm apart from its end (F2) for each time-lapse image. The values were imported into Microsoft Excel, and F1/F2 ratio and changes of MT length were calculated for a plot.

Treatment of Cells with Various Reagents

To disassemble MTs, cultured cells were incubated with 33 μM nocodazole (Sigma) at room temperature, whereas 100 nM nocodazole (Vasquez et al., 1997) or 500 nM taxol (Nakarai Tesque) was used to suppress assembly/disassembly dynamics of plus ends of MTs without decreasing polymer mass or altering MT arrangements.

For permeabilization of cells, cells cultured on glass-bottomed dishes were washed briefly with 70% Dulbecco's PBS(+), and rinsed in the permeabilization buffer (20 mM Hepes, pH 7.3, 110 mM potassium acetate, 2 mM magnesium acetate, 1 mM EGTA, 2 mM DTT, and 0.1 mM PMSF). Cells were then extracted with permeabilization buffer containing 35 μg/ml digitonin, which had been diluted immediately before use, 10 μM taxol and protease inhibitor cocktail (1 mg/ml leupeptin, 1 mg/ml aprotinin, and 1 mg/ml pepstatin) for 5 min at room temperature. After washing with permeabilization buffer containing 10 μM taxol and protease inhibitor cocktail, the dishes were filled with 1 ml of the same buffer. ATP or 5′-adenylylimidodiphosphate (AMP-PNP; Nakarai Tesque) diluted in 100 μl of the same buffer was added to a final concentration of 0.2 mM or 1 mM, respectively, during time-lapse recording (see Fig. 8).

Immunoelectron Microscopy

Cells cultured on collagen-coated dishes were permeabilized with 53 μg/ml digitonin in permeabilization buffer containing 10 μM taxol and protease inhibitor cocktail at room temperature for 10 min. Cells were then washed with the same buffer and fixed with 3.7% formaldehyde at room temperature for 1 h. After washing in Dulbecco's PBS(−), cells were incubated with rabbit anti-GFP pAb for 3 h. Samples were washed several times and then incubated with 5-nm gold-conjugated anti-rabbit IgG antibody (Amersham) for 4 h. Cells were then carefully scraped off the dishes and collected by centrifugation. The pellets were fixed with 2% formaldehyde and 2.5% glutaraldehyde in 0.1 M cacodylate buffer (pH 7.3) followed by post-fixation with 1% OsO_4. Samples were embedded in Epon, and ultrathin sections were cut with a diamond knife, doubly stained with 4% uranyl acetate and 0.4% lead citrate, and viewed with a JEM1010 transmission electron microscope (JEOL). Electron micrographs were digitized with a FILM SCANNER (Nikon; LS-4500AF).

Online Supplemental Material

Seven video files (see below) corresponding to Figs. 5 a; 6, a–c; 7, b and c; and 8 c are available through the JCB online (http://www.jcb.org/cgi/content/full/148/3/505/DC1). QuickTime videos with a longer time duration are also available at http://www.tsukita.jst.go.jp/kiyosue/apc.html. Time-lapse images collected using DeltaVision were processed with Adobe Photoshop software, and converted to QuickTime videos (JPEG compression) with software installed on a Silicon Graphics O2 computer. All videos contain the time-lapse images from the first to the last panel in the corresponding figures. In the videos for Figs. 6 c and 7, b and c, the areas represented in the printed figures are boxed in the first frame of the video.

Fig. 5 a Video. A6 transfectants expressing fAPC-mGFP (green) were stained with PKH26 (red), and images of cells were recorded from 15 min after replating at 1-min intervals. The GFP signal was gradually concentrated at extending cell edges.

Fig. 6 a Video. Time-lapse images of a cell expressing fAPC-GFP (clone A1) were collected at 5-s intervals. Note the clear visualization of a MT itself by fAPC-GFP labeling, the dynamic movement of APC granular structures around MT ends, and the flow of fAPC-GFP signals along the MT.

Fig. 6 b Video. Time-lapse images of a cell transiently expressing fAPC-mGFP were collected at 5-s intervals. Note the dynamic movement of APC granular structures around MT ends.

Fig. 6 c Video. Time-lapse images of a cell expressing fAPC-GFP (clone B4) were collected at 5-s intervals. Note the flow of fAPC-GFP signals along MTs.

Fig. 7 b Video. Time-lapse images of a cell expressing GFP-cAPC were collected at 5-s intervals. GFP-cAPC was concentrated at growing MT ends.

Fig. 7 c Video. Images were collected at 5-s intervals. The cell expressing GFP-cAPC was treated with a low concentration of nocodazole at the timing of 9th frame (indicated in the video) to perturb dynamics of MT plus ends. The concentration of GFP-cAPC at MT ends disappeared within 1 min.

Fig. 8 c Video. Time-lapse images of a cell transiently expressing ΔcAPC-GFP were collected at 5-s intervals. In the cellular extension directing toward the bottom of the image, GFP-positive granular structures moved linearly toward the cell edge.

Results

Expression Level of GFP-tagged Full-Length APC in Cultured A6 Cells

A GFP-tagged *Xenopus* APC protein (APC), fAPC-GFP, in which GFP was fused to the COOH terminus of full-length APC protein (Fig. 1), was constructed, and introduced into *Xenopus* A6 epithelial cells. Three independent clones stably expressing fAPC-GFP were then isolated (Fig. 2). The COOH-terminal -TSV motif of APC was reported to directly bind to the PDZ domain of *hdlg* (Matsumine et al., 1996), suggesting that the fusion of GFP to the COOH terminus of APC in fAPC-GFP affects its

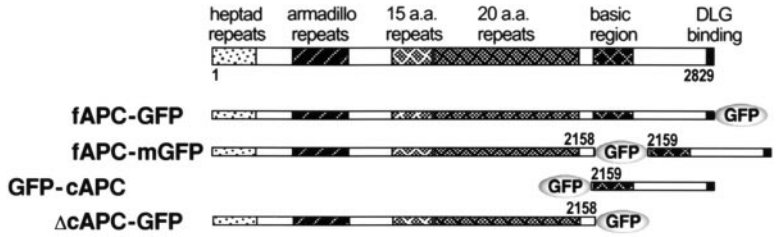

Figure 1. Structures of GFP fusion proteins with full-length APC and deletion mutants of APC. *Xenopus* APC (2829 aa) was tentatively divided into two portions: COOH-terminal (aa 2159–2829) and the remaining portions (aa 1–2158). Based on these portions, two deletion mutants of APC were constructed and fused with GFP. The numbers indicate the amino acid positions.

binding ability to *hdlg*. Therefore, we constructed GFP-fAPC, in which GFP was fused to the NH_2 terminus of full-length APC protein, but for unknown reasons, its expression was not detected by either fluorescence microscopy or immunoblotting in A6 transfectants. Then, we constructed another type of APC-GFP fusion protein, fAPC-mGFP, in which GFP was inserted between the 20-aa repeats and basic region of APC (Fig. 1), and obtained three independent A6 cell clones stably expressing fAPC-mGFP (Fig. 2).

In these stable clones, we examined the degree of overexpression of fAPC-GFP and fAPC-mGFP relative to endogenous APC. Since both endogenous and exogenous APC proteins exhibited fairly broad bands in SDS-PAGE, it was very difficult to resolve these two bands by immunoblotting from the total cell lysate of transfectants. However, when the cell lysate was treated with λ-protein phosphatase before SDS-PAGE, these bands converged to form relatively sharp bands, which allowed quantitative comparison between endogenous and exogenous APC proteins by immunoblotting. As shown in Fig. 2, the ratios of exogenous APC/endogenous APC in transfectants were distributed from ~1 to ~25. For the time-lapse microscopic observation, we mainly used A1 clone of fAPC-GFP-expressing cells (ratio = 3.3) and C1 clone of fAPC-mGFP-expressing cells (ratio = 2.7), and no significant difference was detected between these two clones in terms of the dynamic behavior of APC-GFP fusion proteins along MTs in live cells.

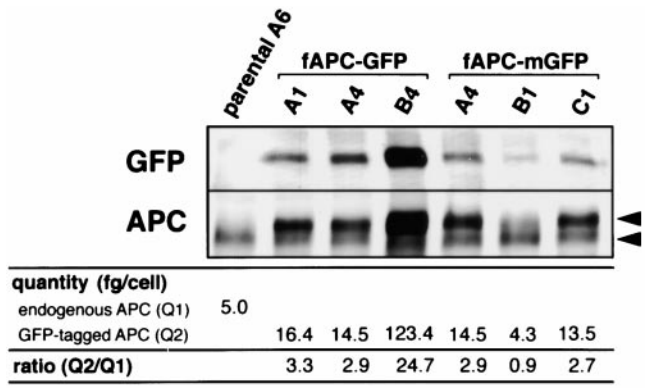

quantity (fg/cell)							
endogenous APC (Q1)	5.0						
GFP-tagged APC (Q2)		16.4	14.5	123.4	14.5	4.3	13.5
ratio (Q2/Q1)		3.3	2.9	24.7	2.9	0.9	2.7

Figure 2. Expression levels of endogenous APC and exogenous GFP-tagged full-length APC. To separate the band of endogenous APC (lower arrowhead) from that of exogenous GFP-tagged APC (upper arrowhead), cell lysates of parental A6 cells and stable clones (A1, A4, and B4 for fAPC-GFP–expressing transfectants, and A4, B1, and C1 for fAPC-mGFP–expressing transfectants) were preincubated with λ-protein phosphatase followed by SDS-PAGE and immunoblotting with anti-GFP pAb (GFP) or anti-APC mAb, APC(Ab-1), (APC). In each lane, the cell lysate from 1×10^6 cells was applied. The amount of endogenous APC in parental A6 cells (Q1) and GFP-tagged APC in stable clones (Q2) were quantified as described in Materials and Methods, and their Q2/Q1 ratios were calculated.

Subcellular Distribution of GFP-tagged Full-Length APC in Cultured A6 Cells

In parental A6 cells, immunofluorescence microscopy revealed that endogenous APC proteins were concentrated along distal end segments of MTs at the tip regions of cellular extensions (Fig. 3 a), similarly to APC proteins in MDCK cells (Näthke et al., 1996). Then, A6 transfectants expressing fAPC-GFP (clone A1; see Fig. 2) were fixed and immunofluorescently stained with mouse anti-tubulin mAb (Fig. 3, b and c). At lower magnification, the distribution of fAPC-GFP was restricted to the tip regions of some cellular extensions (Fig. 3 b). In these tip regions, fAPC-GFP appeared to be associated with MTs to form thick bundles (insets in Fig. 3 b). In thin lamellae of these cells, where MTs spread out toward cellular edges, fAPC-GFP was concentrated at the distal ends of individual microtubules as granules, although some weak GFP signals were also detected diffusely along MTs (Fig. 3 c). These features of the subcellular localization of fAPC-GFP shown in Fig. 3, b and c, were very similar to those of endogenous APC proteins in Fig. 3 a. These findings indicated that fAPC-GFP (and also fAPC-mGFP) is very useful to trace the dynamic behavior of APC in live cells.

Before examination of the dynamic behavior of APC in live cells, fAPC-GFP condensed around MTs was observed by immunoelectron microscopy in A6 transfectants expressing large amounts of fAPC-GFP (clone B4; see Fig. 2). In this clone, at the immunofluorescence microscopic level, fAPC-GFP was detected along the entire length of a subset of MTs, and the fAPC-GFP-associated MTs showed a tendency to be bundled and to run into the cellular extensions, the tips of which showed concentration of fAPC-GFP (data not shown). For immunoelectron microscopy, expressed fAPC-GFP was labeled with anti-GFP pAb after permeabilization of cells with digitonin (Fig. 4). As shown in Fig. 4 a, abnormal thick bundles of MTs were occasionally seen to run through the cytoplasm, and their surfaces were specifically and heavily labeled with immunogold particles. Close inspection revealed that in these bundles parallel MTs were embedded in fuzzy matrices (Fig. 4, b and c). Single MTs decorated by these fuzzy structures were also observed in association with thick bundles (Fig. 4 d) or as scattered structures in the cytoplasm (Fig. 4, e and f). These fuzzy structures, but not

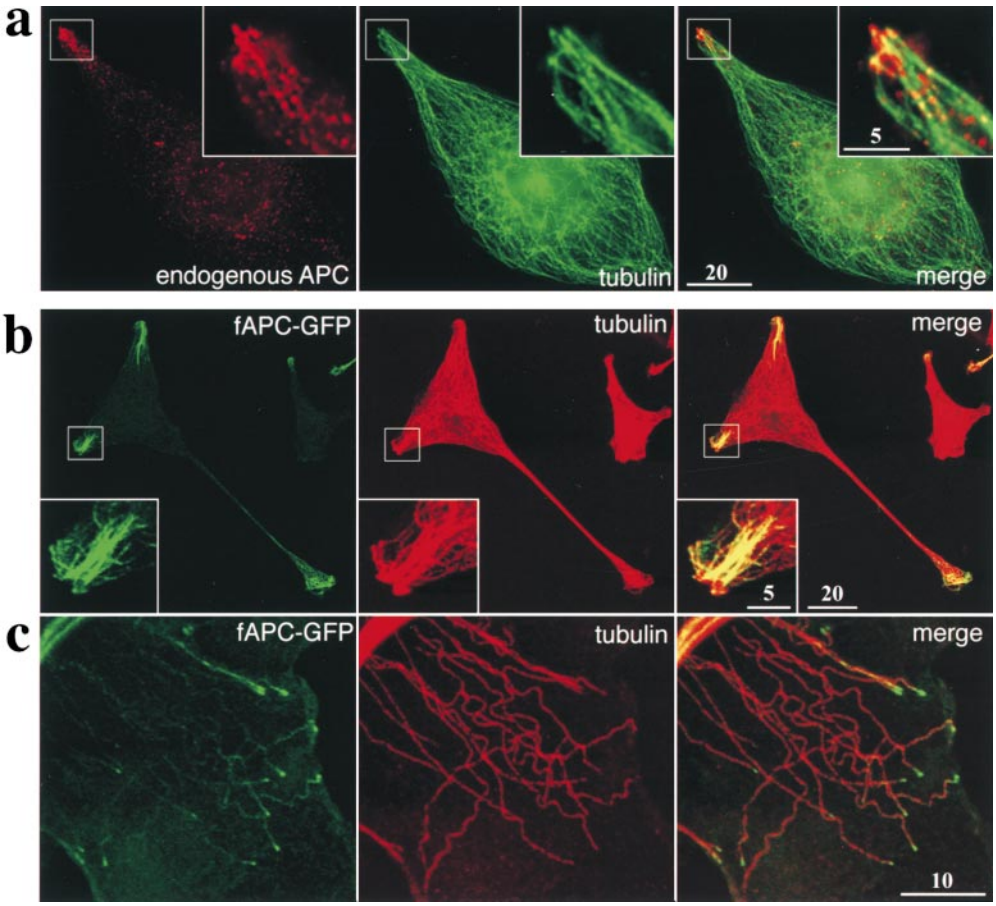

Figure 3. Subcellular distribution of endogenous APC and GFP-tagged full-length APC in stable A6 transfectants. (a) Parental A6 cells were double stained with anti-APC pAb (red) and anti-tubulin mAb (green), and observed with DeltaVision microscope. (b and c) A6 transfectants expressing fAPC-GFP (clone A1; see Fig. 2) were fixed and immunofluorescently stained with anti-tubulin mAb, and observed by confocal microscopy. Expressed fAPC-GFP and MTs were visualized as green and red fluorescence, respectively. In b, fAPC-GFP was concentrated at the tip regions of some cellular extensions, where fAPC-GFP was associated with MTs to form thick bundles (inset). In thin lamellae (c), where MTs spread out toward the cellular edges (toward right), fAPC-GFP was visualized as granules on the distal ends of individual MTs. Note that the subcellular distribution of fAPC-GFP in b was very similar to that of endogenous APC in a. Bars: (a and b) 20 μm; (c) 10 μm; (insets) 5 μm.

MTs per se or membranous structures, were labeled with immunogold particles. Therefore, these findings indicated that these fuzzy structures surrounding MTs were the ultrastructural counterparts for the GFP signals detected in A6 transfectants expressing fAPC-GFP (see Fig. 3).

Dynamic Behavior of GFP-tagged Full-Length APC during Cell Spreading and Wound Healing

We first followed the dynamic behavior of fAPC-mGFP to concentrate at the tip regions in live A6 transfectants (clone C1; see Fig. 2) after replating dissociated cells on glass-bottomed dishes (Fig. 5 a; see video). In trypsinized single cells, the GFP signal was detected as small granules or along filaments, probably MTs (data not shown). At the initial phase of spreading, fAPC-mGFP began to associate with the entire length of radially arranged MTs rather evenly (time 00:00). Within the next several minutes, fAPC-mGFP gradually accumulated around the edges of the cell periphery as granular structures (arrowheads; time 08:09). Subsequently, these GFP-positive granular structures increased in number and began to cluster in several specific regions of the cell periphery (time 20:26). Some of these clusters of APC granular structures continued to grow (arrows), while some disappeared (arrowheads). The emerging of clusters appeared to be associated with the formation/growth of the cellular extensions, resulting in the concentration of the APC granular structures at the tip regions of the extensions (times 34:20–47:43).

Similar polarized clustering of APC granular structures was observed during the process of wound healing. Confluent cultures of A6 transfectants expressing fAPC-mGFP were manually scratched with sharp needles as shown in the phase-contrast image in Fig. 5 b. Within 2 h after wounding, at the front row of the wound, fAPC-mGFP began to gradually concentrate at the distal ends of a subset of MTs, which were laterally associated to form thick bundles (times 00:30:52–02:02:03). These fAPC-mGFP-concentrated MT bundles appeared to continuously grow toward the wounded region (arrows and arrowheads; times 02:02:03–02:49:07).

These findings as well as images shown in Figs. 3 and 4 suggested that the peculiar polarized behavior of APC is dependent on MTs. Then, A6 transfectants expressing fAPC-mGFP were treated with a high concentration of nocodazole (33 μM) to disassemble MTs, and at 10-, 30-min, or 3-h incubation, cells were fixed and immunofluorescently stained with anti-tubulin mAb (Fig. 5 c). At 10-min incubation, almost all MTs in the cell periphery were disassembled (time 10 min). However, the APC granular structures remained localized at the original positions, i.e., the tip regions of cellular extensions, and were clustered at the level of the basal plasma membrane cortex. These granular structures gradually moved toward the center of

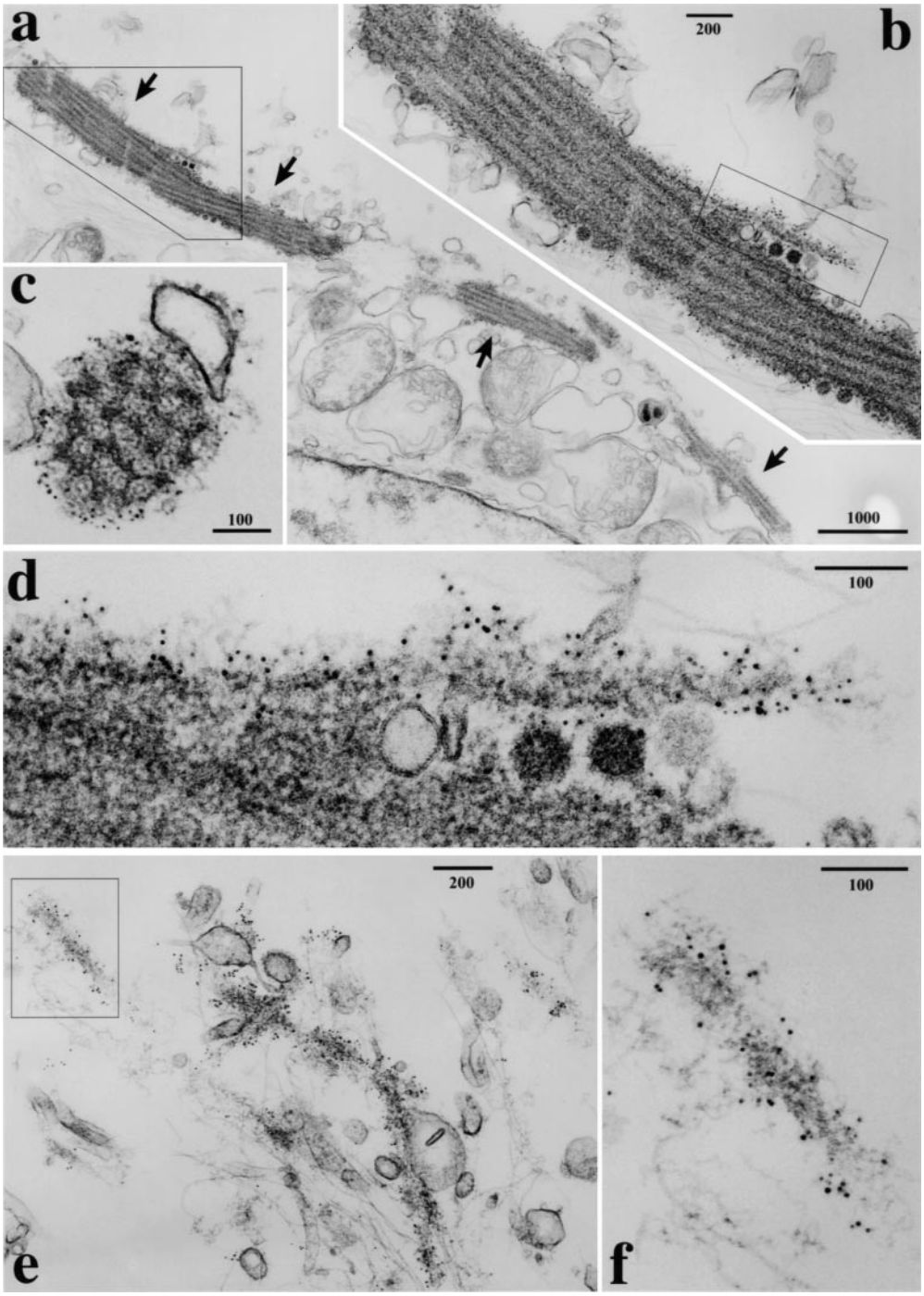

Figure 4. Immunolabeling of fAPC-GFP aggregates with anti-GFP pAb in A6 transfectants at the electron microscopic level. A6 transfectants expressing large amounts of fAPC-GFP (clone B4; see Fig. 2) were permeabilized with digitonin and incubated with rabbit anti-GFP pAb, followed by incubation with 5-nm gold-conjugated anti-rabbit IgG pAb. Abnormal thick bundles of MTs were occasionally observed (arrows in a). Boxed areas in a, b, and e were enlarged in b, d, and f, respectively. Both longitudinal (b) and transverse (c) sectional images of these thick MT bundles revealed that in these bundles, MTs were embedded in fuzzy matrices, which were directly labeled with anti-GFP pAb. Single microtubules surrounded by immunolabeled fuzzy structures were also occasionally observed (d–f). Note that no membranous vesicles were labeled with immunogold particles. Bars: (a) 1,000 nm; (b and e) 200 nm; (c, d, and f) 100 nm.

cells (~0.4 μm/min) remaining at the level of the basal plasma membrane cortex (time 30 min), and were finally distributed along the central portion of the basal plasma membrane cortex in a striped pattern (time 3 h). This pattern was complementary with that of rhodamine phalloidin-stained stress fibers (data not shown). Taking into consideration that the plasma membrane cortex continuously moves rearward in the migrating lamellae and lamellipodia (reviewed in Mitchison and Cramer, 1996), when MTs were disassembled, these APC granular structures would be relocated by this rearward transport in association with the basal plasma membrane cortex. Therefore, these findings suggested that APC bound to both MTs and plasma membrane cortex, and that these interactions are required for the peculiar polarized behavior of APC in live cells.

Dynamic Behavior of GFP-tagged Full-Length APC at the Distal Ends of Microtubules

Next, we examined the dynamic behavior of fAPC-GFP or fAPC-mGFP at the distal ends of MTs at higher magnification with shorter time intervals in live cells. Fig. 6 a shows a series of time-lapse images of the GFP signal (fAPC-GFP) in a lamella traveling toward the left (clone

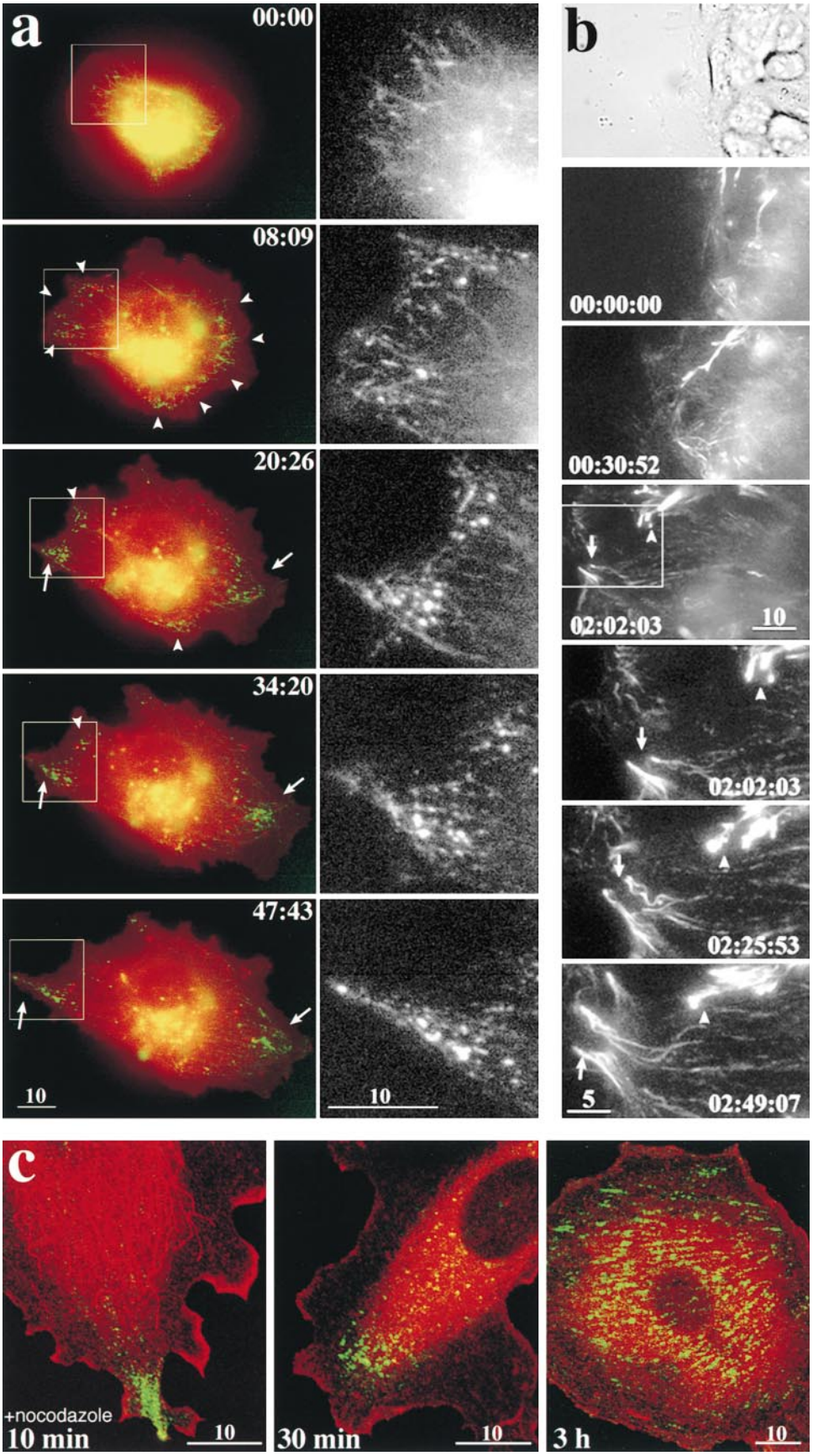

Figure 5. The behavior of full-length APC in live cells (clone C1; see Fig. 2) during cell spreading and wound healing. (a) A6 transfectants stably expressing fAPC-mGFP were replated on glass-bottomed dishes, and a series of fluorescence microscopic images were obtained. The aggregates of fAPC-mGFP were visualized as green fluorescence. Plasma membranes of these cells were labeled with PKH26 in red (some endocytotic vesicles were also labeled in red). Cells were replated 1 h after trypsinization and recording of the images was started 15 min after replating. Only the GFP signal in boxed areas in color plates were selected in corresponding black-and-white plates at larger magnification. See details in the text. Elapsed time was indicated at top right (in min:s). QuickTime video is available at http://www.jcb.org/cgi/content/full/148/3/505/DC1. (b) Confluent cultures of A6 transfectants expressing fAPC-mGFP were manually scratched with sharp needles. The top panel shows a phase-contrast image of cells at the edge of the wound shortly after wounding. Second to fourth panels (times 00:00:00–02:02:03) show fluorescence images of fAPC-mGFP with the same scale and position as the top phase-contrast panel. Fifth to last panels (times 02:02:03–02:49:07) show a series of magnified images of the boxed area in the fourth panel. See details in the text. Elapsed time is indicated at the bottom (in h:min:s). (c) A6 transfectants expressing fAPC-mGFP were incubated with 33 μM nocodazole to disassemble MTs for 10 min, 30 min, and 3 h, then fixed and immunofluorescently stained with anti-tubulin mAb in red. The fAPC-mGFP was visualized as green fluorescence. See details in the text. Bars: (a, b, top, and c) 10 μm; (b, bottom) 5 μm.

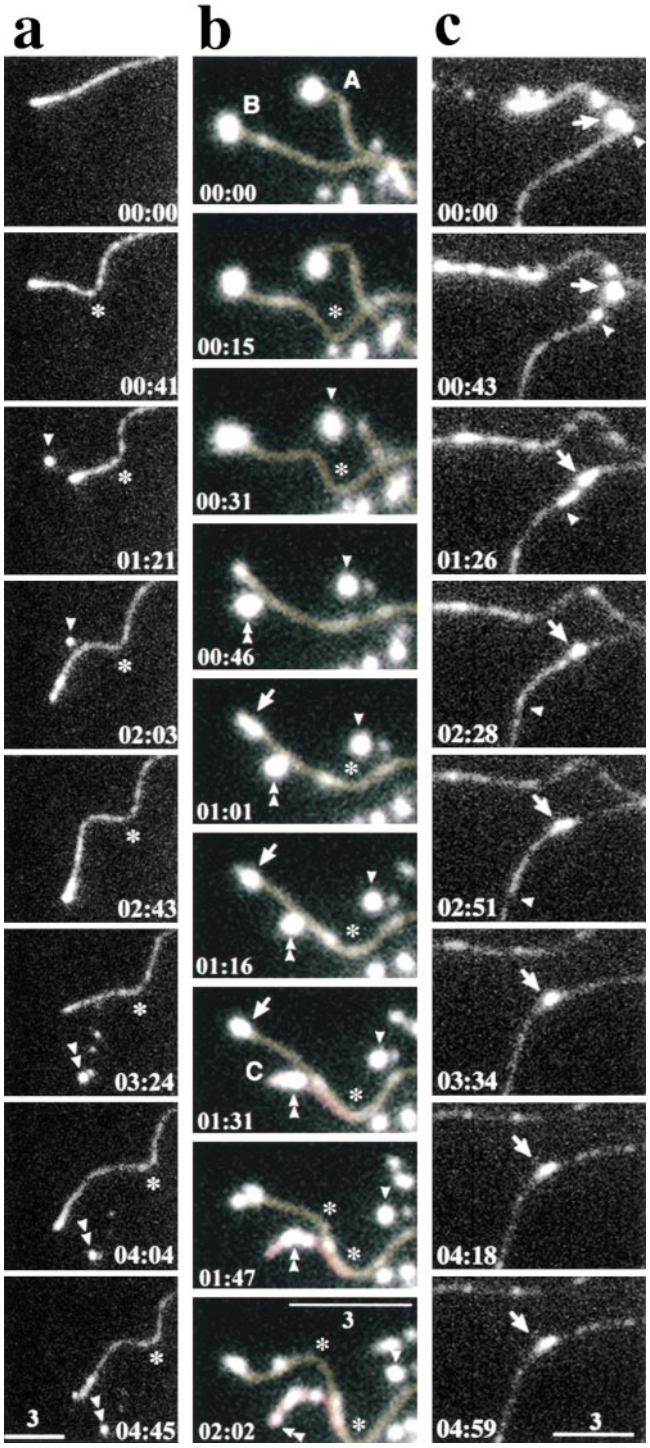

Figure 6. The behavior of full-length APC in live cells at the distal ends of MTs. (a and b) A series of time-lapse images was obtained from a thin lamella of a A6 cell expressing fAPC-GFP (clone A1; see Fig. 2) or fAPC-mGFP (transient expression), respectively. In these thin lamellae, individual MTs were spread out toward the leading edge of the cell, which was directed to the left. Since GFP-tagged molecules were not only concentrated at the distal ends of MTs but also evenly covered individual MTs, imaging only by GFP fluorescence allowed us to observe the dynamic behavior of fAPC-GFP/fAPC-mGFP as well as MTs simultaneously. Asterisks and arrowheads indicate the rearward movement of the bending points of MTs and the granules dropped off from shortening MT ends, respectively. See details in the text. Microtubule-A/B and -C in b were colored in yellow and pink on the computer, respectively. (c) Another series of time-lapse images of clone B4 (see Fig. 2) showing the continuous flow of fAPC-GFP along MTs (arrows and arrowheads) toward their distal ends. This continuous flow is clearly visualized in the video. In a–c, elapsed time is indicated at bottom (in min:s). QuickTime videos for a–c are available at http://www.jcb.org/cgi/content/full/148/3/505/DC1. Bars: 3 μm.

A1; see Fig. 2; see video). Since fAPC-GFP was not only concentrated at the tips of MTs but also diffusely covered the distal segments of these MTs (see Fig. 3 c), imaging only by the GFP fluorescence allowed to observe the dynamic behavior of fAPC-GFP as well as MTs simultaneously. In this series of time-lapse images, MT itself was continuously transported rearward (toward the right) in the lamellae (Mikhailov and Gundersen, 1995; Waterman-Storer and Salmon, 1997), resulting in the under- and overestimation of the growth and shortening rates of the distal end of MT, respectively. (Note the rearward movement of MT marked by asterisks.) When this MT continued to grow (times 00:00–00:41, 01:21–02:43, and 03:24–04:45), fAPC-GFP was gradually accumulated as granules at the tip of MT. During this series, this MT switched from the growth to the shortening phase twice (times 00:41–01:21 and 02:43–03:24), and concomitantly the APC granules dropped off from MT. This granules did not diffuse away into the cytoplasm, but continuously moved rearward (arrowheads). The shortening MT was free from the APC concentration on its end. Interestingly, when growing MT passed by the APC granule that had been dropped from MT (arrowhead; time 02:03), this granule was reloaded onto MT and moved toward its plus end (see video). Similar behavior of APC granules was more clearly observed in A6 transfectants transiently expressing relatively large amounts of fAPC-mGFP (Fig. 6 b; see video). When MT-A and -B continued to grow (times 00:00–00:15 and 00:00–00:31, respectively), fAPC-mGFP was concentrated as granules on the tips of MTs. When these MTs switched from the growth to the shortening phase, the APC granules dropped off from MTs. These granules continuously moved rearward (arrowheads).

In the series of Fig. 6 a, some continuous flow of the GFP signals along MTs toward their distal ends was clearly detected (see video). This flow of APC was more clearly visualized in A6 transfectants expressing relatively large amounts of fAPC-GFP (clone B4; see Fig. 2; Fig. 6 c, see video). Therefore, we were led to conclude that APC molecules move continuously on the surface of a subset of MTs toward plus ends, and that only when MTs are growing they accumulate at their plus ends as granules. To further understand this peculiar and complicated behavior of APC molecules, we next constructed GFP-tagged deletion mutants of APC (see Fig. 1), and examined their dynamic behavior in live A6 cells.

Concentration of COOH-terminal Segment of APC at Growing Ends of Microtubules

Since the COOH-terminal 671 amino acids sequence contained the MT-binding domain of APC in vitro (aa 2219–2580 of human APC; Deka et al., 1998), we constructed

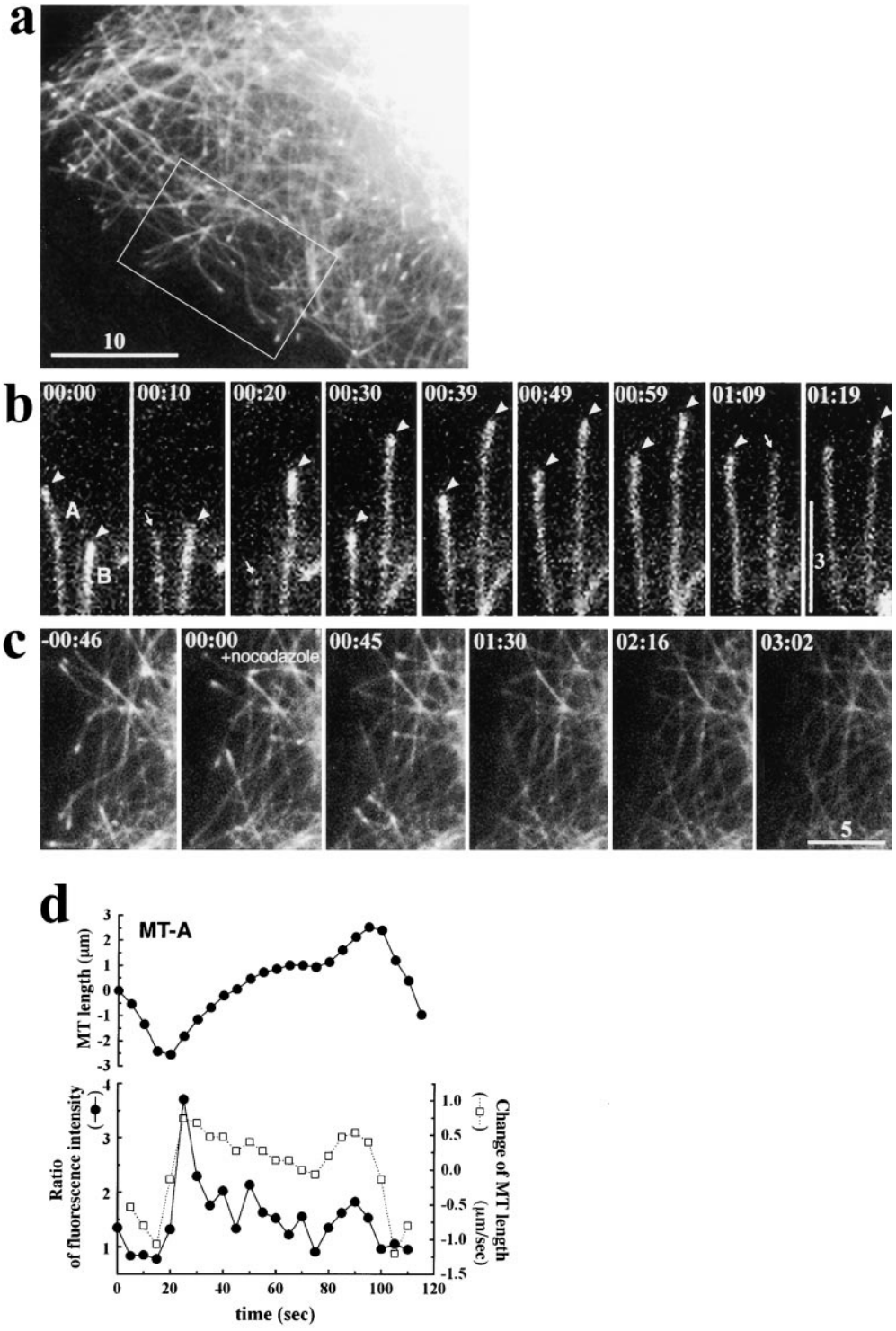

Figure 7. The behavior of the COOH-terminal region of APC in live cells. A6 cells transiently expressing GFP-cAPC (see Fig. 1) were observed. (a) In A6 cells expressing relatively low level of GFP-cAPC, GFP-cAPC was distributed along the entire length of all MTs, but was significantly concentrated at the distal ends of MTs. (b) The dynamic behavior of GFP-cAPC at the distal ends of two MTs (A and B) in the lamellae, which was directed to the top. Only when these MTs continued to grow, the distal ends of MTs were highlighted by the GFP signal (arrowheads). When MTs were switched from growth to shortening phase, the GFP-cAPC concentrated at ends of MTs abruptly disappeared (arrows). (c) Effects of low concentration of nocodazole (100 nM), which affects the assembly/disassembly dynamics of MTs at their plus ends without changing their polymer mass, on the behavior of GFP-cAPC at the ends of MTs. The boxed area in a was enlarged in c. Within 1-min incubation with nocodazole, the concentration of GFP-cAPC at MT ends became undetectable, leaving evenly distributed GFP-cAPC along the entire length of MTs. (d) Quantitative analyses of the relationship between the length of MT-A and the degree of concentration of GFP-cAPC on their ends in b. The upper panel is a plot of MT length and the lower panel represents changes of MT length (open squares; right-hand scale) and the ratios of fluorescence intensities between the MT end and the proximal segments (closed circles, left-hand scale; see Materials and Methods). This quantification clearly showed the specific association of the GFP-cAPC concentration with growing MTs but not with shortening MTs. Elapsed time is indicated at top left (in min:s). Bars: (a) 10 μm; (b) 3 μm; (c) 5 μm. QuickTime videos for b and c are available at http://www.jcb.org/cgi/content/full/148/3/505/DC1.

cDNA encoding this region with a GFP tag at its NH_2 terminus (GFP-cAPC; see Fig. 1), introduced it into A6 cells, and observed transfectants transiently expressing GFP-cAPC. In A6 cells expressing relatively low levels of GFP-cAPC, weak GFP signals were detected along the entire length of all MTs with significant concentration of signals at the distal ends of MTs (Fig. 7 a). When these cells were observed as a video, the concentration of GFP signals on MT ends moved for some distance followed by abrupt disappearance. Fig. 7 b shows a series of time-lapse images indicating dynamic growth and shortening of two MTs (MT-A and -B) in these cells. Only when these MTs con-

tinued to grow, the distal ends of MTs were highlighted by the GFP signal (arrowheads). When MTs were switched from growth to shortening phase, the concentration of GFP-cAPC at ends of MTs abruptly disappeared (arrows). These findings suggested that the concentration of GFP-cAPC was associated only with the growing ends of MTs. In Fig. 7 d, the degree of concentration of GFP-cAPC on MT-A was quantitatively represented as the ratio of fluorescence intensity between the end segment and the following segment of MTs. This quantification clearly showed the specific association of the GFP-cAPC concentration with growing MTs but not with shortening MTs. To further confirm this specific association, cells were treated with a low concentration of nocodazole (100 nM) to block the assembly/disassembly dynamics of MTs at their plus ends without changing their polymer mass (Vasquez et al., 1997). Within 1-min incubation with nocodazole, the concentration of GFP-cAPC at MT ends became undetectable, leaving an even distribution of GFP-cAPC along the entire length of MTs (Fig. 7 c; see video). Low concentration of taxol (500 nM) also showed the same effect on the behavior of GFP-cAPC.

Active Transport of APC Mutant Lacking Its COOH-terminal Region along Microtubules toward Their Plus Ends

We next examined the subcellular distribution and the dynamic behavior of the APC mutant lacking its COOH-terminal MT-binding domain with a GFP tag at its COOH terminus, ΔcAPC-GFP, in live A6 cells (see Fig. 1). First, A6 transfectants expressing ΔcAPC-GFP were fixed and immunofluorescently stained with anti-tubulin mAb (Fig. 8 a). Expressed ΔcAPC-GFP formed granular structures scattered around the cytoplasm with various diameters. Interestingly, these granules occasionally clustered in the tip region of some of the cellular extensions similarly to fAPC-mGFP (see Fig. 3). In thin lamellae, it was clear that these granules were aligned along MTs (Fig. 8 b), indicating that ΔcAPC-GFP lacking the conventional MT-binding site could still interact with MTs directly or indirectly. This type of MT-associated distribution of ΔcAPC-GFP was observed clearly up to 1 day after cells were replated.

When these cells were observed by time-lapse microscopy at low magnification, the ΔcAPC-GFP granules were seen to continuously move toward the cell periphery. Fig. 8 c shows one series of time-lapse images indicating the movement of these granules at higher magnification (see video). Since, differently from fAPC-mGFP and GFP-cAPC, ΔcAPC-GFP did not decorate MTs diffusely, MTs were not visible in these images, but a large granule was found moving linearly toward the tip of cellular extensions over a long period (arrowheads). During the course of traveling to the tip, granules occasionally changed their shapes, divided into smaller fragments, or fused to each other, suggesting that they have a flexible liquid-like nature. Their movements were predominantly unidirectional with a peak velocity of ~10 μm/min. When cells were treated with 33 μM nocodazole to disassemble MTs, the movements of the granules became vibrational with no net translocation (data not shown). These observations suggested that the ΔcAPC-GFP granules move along MT tracks. Then, to check the ATP dependency, the movement of these ΔcAPC-GFP granules was examined in permeabilized A6 transfectants (Fig. 8 d). Permeabilization with digitonin did not affect the shape of granules, but completely stopped their directional movement. When these permeabilized cells were incubated with 0.2 mM ATP, the movement of some granules was induced. The ΔcAPC-GFP granules moved unidirectionally and linearly toward the tips of cellular extensions (arrows; times −01:50–01:45). When 1 mM AMP-PNP, a nonhydrolyzable analogue of ATP, was added, the movement stopped within a minute (arrowheads; times 01:45–05:35). These findings indicated that the motility of the ΔcAPC-GFP granules requires ATP hydrolysis.

APC was reported to form dimers through its NH_2-terminal α-helical coiled-coil region (Joslyn et al., 1993; Su et al., 1993a). Therefore, it was possible that ΔcAPC-GFP bound to endogenous APC to form heterodimers in A6 transfectants, and that endogenous APC in the heterodimers mediated the localization and movement of ΔcAPC-GFP. However, when A6 transfectants expressing ΔcAPC-GFP were stained with a pAb against COOH-terminal peptide of APC, in the tip region of cellular extensions only a small number of the GFP-positive granules (3–4%) were stained with this pAb (not shown). Therefore, it is likely that the subcellular localization and the dynamic behavior of ΔcAPC-GFP observed in this study was attributable to the intrinsic nature of ΔcAPC-GFP itself.

Discussion

This is essentially a descriptive study, in which the localization of GFP-tagged APC molecules was detected in live *Xenopus* A6 epithelial cells. In this description, we first reported the peculiar dynamic behavior of GFP-APC molecules within cells. It is reasonable to consider that this behavior of GFP-tagged full-length APC can be regarded as that of endogenous APC, partly because the expression level of GFP-APC was approximately threefold that of endogenous APC (see Fig. 2), and partly because the subcellular localization of GFP-APC was very similar to that of endogenous APC in fixed cells at the immunofluorescence microscopic level (see Fig. 3). Immunoelectron microscopy revealed the expressed GFP-tagged full-length APC as fuzzy structures decorating MTs (see Fig. 4). Observations in live cells (see Fig. 6 and corresponding videos) uncovered the following behavior of GFP-tagged full-length APC; (a) these GFP-APC-based fuzzy structures move in a stream along a subset of MTs toward their plus ends, (b) when GFP-APC molecules arrived at the plus ends of growing MTs, these molecules remain and accumulate at the ends to form granular structures, (c) when MTs began to shorten, these GFP-APC granules dropped off from the ends of MTs, maintaining their structural integrity, and (d) these APC granules were occasionally reloaded onto the same or another MT that passed by the granules. Through these behaviors, APC granules appeared to be transported to and accumulated at the tip regions of the cellular extensions. This concentration of APC was previously reported by conventional immunofluorescence microscopy (Näthke et al., 1996).

The molecular mechanism behind this peculiar behavior

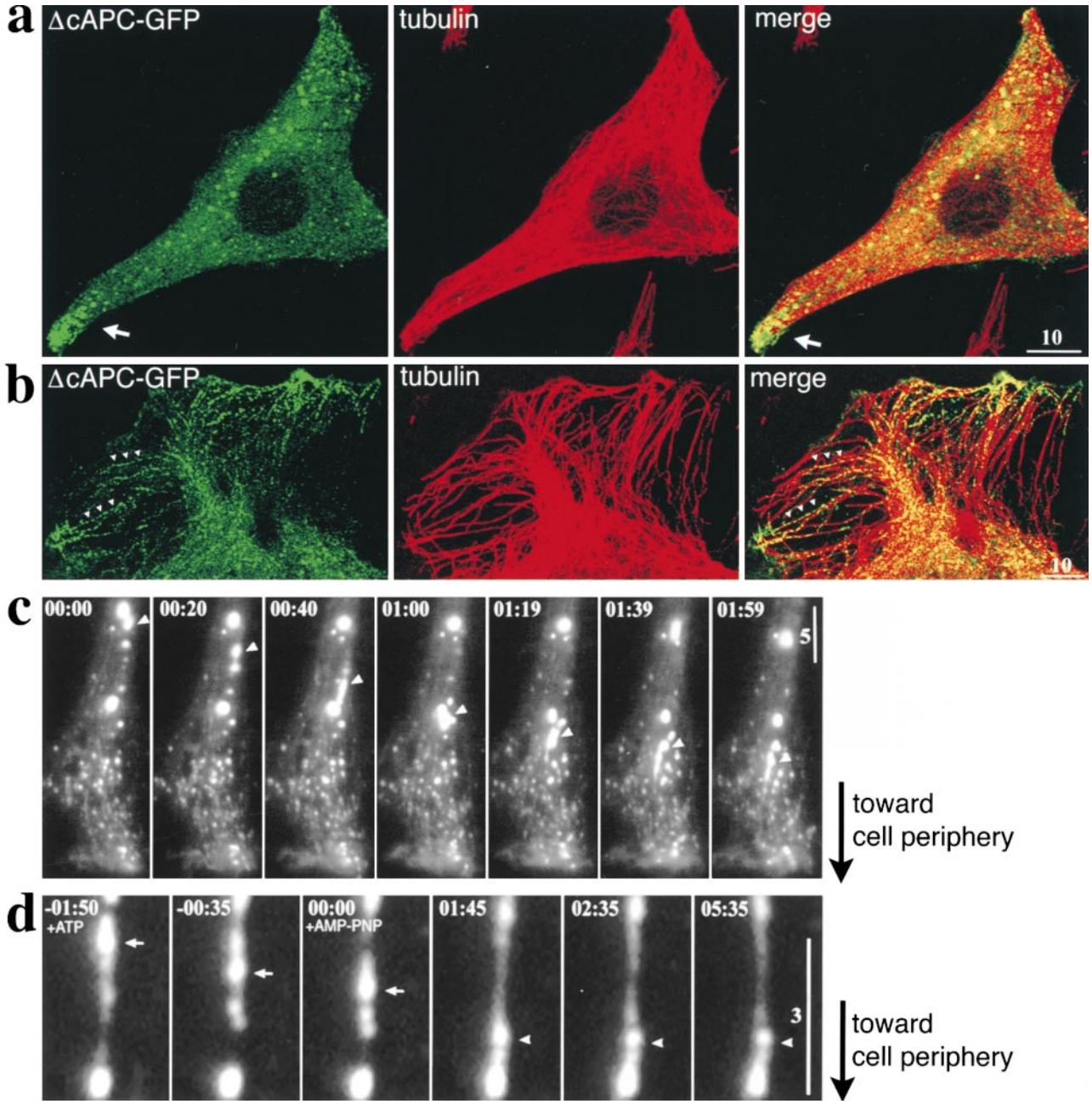

Figure 8. Subcellular distribution and the behavior of the deletion mutant of APC lacking its COOH-terminal region in A6 transfectants. (a and b) A6 cells expressing ΔcAPC-GFP (see Fig. 1) were fixed and stained with anti-tubulin mAb in red. Expressed ΔcAPC-GFP formed granular structures (green) with various diameters scattered around the cytoplasm. These granules occasionally clustered in the tip region of some, but not all, of the cellular extensions (arrows in a). In thin lamellae (b), these granules were shown to be aligned along MTs (arrowheads in b). (c) A series of time-lapse fluorescence images was obtained from cellular extensions of live A6 cells expressing ΔcAPC-GFP. Since, differently from fAPC-mGFP and GFP-cAPC, ΔcAPC-GFP did not decorate MTs, MTs were not visible in these images. A large granule moving linearly toward the cell edge is indicated by an arrowhead. A QuickTime video is available at http://www.jcb.org/cgi/content/full/148/3/505/DC1. (d) Movements of the ΔcAPC-GFP granules in permeabilized cells. A6 cells expressing ΔcAPC-GFP were replated, cultured for 4 h, and then permeabilized with digitonin in the presence of 10 μM taxol. Addition of 0.2 mM ATP induced linear movements of the granules toward the cell periphery (times −01:50–01:45, arrows). Further addition of 1 mM AMP-PNP at time 00:00 blocked these movements (times 01:45–05:35, arrowheads). Elapsed time is indicated at top left (in min:s). Bars: (a and b) 10 μm; (c) 5 μm; (d) 3 μm.

of APC remains unclear, but the present observations on the behavior of GFP-cAPC and ΔcAPC-GFP (see Fig. 1) in live cells provide clues to understanding the mechanism. Similar to full-length APC, GFP-cAPC were also concentrated at the distal ends of growing MTs in live cells (see Fig. 7), but there were several clear differences in their manner of concentration. First, continuous flow of the full-length APC was observed on MTs toward their distal ends

(see Fig. 6, a and c), whereas such flow was not detected for GFP-cAPC (see Fig. 7 c). Second, when MTs were upon transition from growth to the shortening phase, the full-length APC granular structures at the ends of MTs dropped off from MTs, while maintaining granular structural integrity (see Fig. 6, a and b), whereas the GFP-cAPC concentrated at the ends of MTs abruptly disappeared (see Fig. 7 b). GFP-cAPC did not accumulate at MT ends as large granular structures. When MTs were totally disassembled with nocodazole (33 μM), GFP-cAPC was distributed diffusely in the cytoplasm without forming detectable granular structures, and was easily extracted by treatment with digitonin (data not shown). These findings suggested that, in contrast to full-length APC, GFP-cAPC molecules are associated with MTs without forming aggregates under the equilibrium with a soluble pool of GFP-cAPC in the cytoplasm.

The behavior and characteristics of GFP-cAPC are very similar to those of CLIP-170, which was recently reported using the GFP-CLIP170 fusion protein (Perez et al., 1999). CLIP-170 was first identified as a microtubule-associated protein (MAP) in HeLa cells (Rickard and Kreis, 1990), and time-lapse analyses with GFP-CLIP170 revealed that CLIP-170 bound to MTs in stretches along their growing ends. Detailed analyses in vivo (Perez et al., 1999) and in vitro (Diamantopoulos et al., 1999) indicated that CLIP-170 treadmills on growing MT ends, i.e., that CLIP-170 is incorporated into MT ends by copolymerizing with free tubulin dimers and released from the older part of MTs. In good agreement with this conclusion, CLIP-170 disappeared from the MT ends when cells were treated with reagents such as low concentrations of nocodazole and taxol that perturb MT dynamics. Interestingly, these reagents also removed the stretches of GFP-cAPC from MT ends (see Fig. 7 c). Therefore, it is likely that GFP-cAPC is preferentially associated with the growing plus ends of MTs by the same molecular mechanism as CLIP-170, although it is not clear whether the GFP-cAPC/MT interaction is direct or indirect. Since EB/RP family proteins interact with the COOH-terminal region of APC (Su et al., 1995; Renner et al., 1997) and are concentrated at ends of a subset of MTs (Morrison et al., 1998; Juwana et al., 1999), it is possible that GFP-cAPC is targeted to the ends of MTs via EB/RP family members.

The behavior of ΔcAPC-GFP was also peculiar (see Fig. 8). In contrast to GFP-cAPC, ΔcAPC-GFP did not decorate MTs, which appeared to be consistent with previous studies that full-length APC interacts with MTs at its COOH-terminal domain (Munemitsu et al., 1994; Smith et al., 1994). Instead, ΔcAPC-GFP formed granular structures in various sizes that were aligned and moved along MTs toward their distal ends in an ATP-dependent manner. These findings clarified two characteristic properties of ΔcAPC. First, ΔcAPC has an ability to aggregate to form polymers. To date, the first 45 amino acids of APC were reported to be necessary for APC dimerization (Joslyn et al., 1993; Su et al., 1993a), but it remains unclear how ΔcAPC as well as full-length APC can aggregate to form large granular structures. Second, ΔcAPC also interacts with MTs. If some kinesin-like motors are postulated to be associated with the ΔcAPC granules, the ΔcAPC/MT interaction as well as the ATP-dependent movement of granules along MTs toward their plus ends can be explained. However, other molecular mechanisms could also be responsible for this interaction and movement, and identification of ΔcAPC-binding proteins as well as in vitro motility analyses are required in the future studies.

In summary, among peculiar behaviors of full-length APC in live cells, its COOH-terminal domain (cAPC) and the remaining portion (ΔcAPC) appear to be responsible for the high affinity to the ends of growing MTs and granular formation as well as translocation along MTs toward the plus ends, respectively. In addition to these behaviors, as shown in Fig. 5, during cell spreading and wound healing, APC granules clustered in specific regions of the cell periphery with concomitant formation of cellular extensions, resulting in the accumulation of APC granules at the tip regions of cellular extensions, i.e., in these cells, a subset of MTs were selected to be decorated by full-length APC. The ability to select MTs appeared to be attributed not to the COOH-terminal domain (cAPC) but to the remaining portion of APC (ΔcAPC); GFP-cAPC labeled all MTs (see Fig. 7), whereas ΔcAPC-GFP granules showed a tendency to concentrate at some cellular extensions (see Fig. 8 a). These findings favor the notion that APC plays some important role in polarized cellular morphogenesis through the stabilization of cellular extensions (Näthke et al., 1996; Barth et al., 1997b; Pollack et al., 1997). Of course, it remains elusive whether the APC-dependent selection of MTs is the cause or result for the stabilization of cellular extensions.

Much attention has been focused on the function of APC that pertains to its ability to regulate β-catenin activity (for reviews see Peifer, 1995; Barth et al., 1997a; Cadigan and Nusse, 1997; Ben-Ze'ev and Geiger, 1998), but the relationship of APC to MT dynamics has been sorely neglected. However, it is reasonable to speculate that APC, in living cells by behaviors as described in detail in this study, accomplishes certain important physiological functions. The present study using GFP-tagged APC molecules provides an advantageous system to analyze the relationship of APC to MT dynamics in situ. This system will allow more detailed analyses not only of the behavior of various GFP-tagged APC mutants within live cells but also of their effects on MT dynamics.

We thank Drs. A. Nagafuchi (Kyoto University) and H. Oda (Tsukita Cell Axis Project) for valuable discussions. Our thanks are also due to Dr. S. Yonemura (Kyoto University) for technical help with electron microscopy, to Dr. A. Asano (Tsukita Cell Axis Project) for critically reading the manuscript, and to all the other members of our laboratory for helpful discussions and technical assistance.

References

Barth, A.I., I.S. Näthke, and W.J. Nelson. 1997a. Cadherins, catenins and APC protein: interplay between cytoskeletal complexes and signaling pathways. *Curr. Opin. Cell Biol.* 9:683–690.

Barth, A.I., A.L. Pollack, Y. Altschuler, K.E. Mostov, and W.J. Nelson. 1997b. NH_2-terminal deletion of β-catenin results in stable colocalization of mutant β-catenin with adenomatous polyposis coli protein and altered MDCK cell adhesion. *J. Cell Biol.* 136:693–706.

Ben-Ze'ev, A., and B. Geiger. 1998. Differential molecular interactions of β-catenin and plakoglobin in adhesion, signaling and cancer. *Curr. Opin. Cell Biol.* 10:629–639.

Bergen, L.G., and G.G. Borisy. 1980. Head-to-tail polymerization of microtubules *in vitro*. Electron microscope analysis of seeded assembly. *J. Cell Biol.* 84:141–150.

Binder, L.I., W.L. Dentler, and J.L. Rosenbaum. 1975. Assembly of chick brain

tubulin onto flagellar microtubules from *Chlamydomonas* and sea urchin sperm. *Proc. Natl. Acad. Sci. USA*. 72:1122–1126.
Cadigan, K.M., and R. Nusse. 1997. Wnt signaling: a common theme in animal development. *Genes Dev*. 11:3286–3305.
Cassimeris, L. 1999. Accessory protein regulation of microtubule dynamics throughout the cell cycle. *Curr. Opin. Cell Biol.* 11:134–141.
Cassimeris, L., N.K. Pryer, and E.D. Salmon. 1988. Real-time observations of microtubule dynamic instability in living cells. *J. Cell Biol.* 107:2223–2231.
Cole, N.B., and J. Lippincott-Schwartz. 1995. Organization of organelles and membrane traffic by microtubules. *Curr. Opin. Cell Biol.* 7:55–64.
Deka, J., J. Kuhlmann, and O. Muller. 1998. A domain within the tumor suppressor protein APC shows very similar biochemical properties as the microtubule-associated protein tau. *Eur. J. Biochem*. 253:591–597.
Desai, A., and T.J. Mitchison. 1997. Microtubule polymerization dynamics. *Annu. Rev. Cell Dev. Biol.* 13:83–117.
Diamantopoulos, G.S., F. Perez, H.V. Goodson, G. Batelier, R. Melki, T.E. Kreis, and J.E. Rickard. 1999. Dynamic localization of CLIP-170 to microtubule plus ends is coupled to microtubule assembly. *J. Cell Biol.* 144:99–112.
Goodson, H.V., C. Valetti, and T.E. Kreis. 1997. Motors and membrane traffic. *Curr. Opin. Cell Biol.* 9:18–28.
Gotlieb, A.I., L.M. May, L. Subrahmanyan, and V.I. Kalnins. 1981. Distribution of microtubule organizing centers in migrating sheets of endothelial cells. *J. Cell Biol.* 91:589–594.
Hulsken, J., W. Birchmeier, and J. Behrens. 1994. E-cadherin and APC compete for the interaction with β-catenin and the cytoskeleton. *J. Cell Biol.* 127: 2061–2069.
Ikeda, S., S. Kishida, H. Yamamoto, H. Murai, S. Koyama, and A. Kikuchi. 1998. Axin, a negative regulator of the Wnt signaling pathway, forms a complex with GSK-3β and β-catenin and promotes GSK-3β-dependent phosphorylation of β-catenin. *EMBO (Eur. Mol. Biol. Organ.) J.* 17:1371–1384.
Joslyn, G., D.S. Richardson, R. White, and T. Alber. 1993. Dimer formation by an N-terminal coiled coil in the APC protein. *Proc. Natl. Acad. Sci. USA*. 90: 11109–11113.
Juwana, J.P., P. Henderikx, A. Mischo, A. Wadle, N. Fadle, K. Gerlach, J.W. Arends, H. Hoogenboom, M. Pfreundschuh, and C. Renner. 1999. EB/RP gene family encodes tubulin binding proteins. *Int. J. Cancer*. 81:275–284.
Kinzler, K.W., and B. Vogelstein. 1996. Lessons from hereditary colorectal cancer. *Cell*. 87:159–170.
Kirschner, M., and T. Mitchison. 1986. Beyond self-assembly: from microtubules to morphogenesis. *Cell*. 45:329–342.
Liao, G., T. Nagasaki, and G.G. Gundersen. 1995. Low concentrations of nocodazole interfere with fibroblast locomotion without significantly affecting microtubule level: implications for the role of dynamic microtubules in cell locomotion. *J. Cell Sci.* 108:3473–3483.
Matsumine, A., A. Ogai, T. Senda, N. Okumura, K. Satoh, G.H. Baeg, T. Kawahara, S. Kobayashi, M. Okada, K. Toyoshima, and T. Akiyama. 1996. Binding of APC to the human homolog of the *Drosophila* discs large tumor suppressor protein. *Science*. 272:1020–1023.
Mikhailov, A.V., and G.G. Gundersen. 1995. Centripetal transport of microtubules in motile cells. *Cell Motil. Cytoskeleton*. 32:173–186.
Mitchison, T.J., and L.P. Cramer. 1996. Actin-based cell motility and cell locomotion. *Cell*. 84:371–379.
Mitchison, T., and M. Kirschner. 1984. Dynamic instability of microtubule growth. *Nature*. 312:237–242.
Morin, P.J., A.B. Sparks, V. Korinek, N. Barker, H. Clevers, B. Vogelstein, and K.W. Kinzler. 1997. Activation of β-catenin-Tcf signaling in colon cancer by mutations in β-catenin or APC. *Science*. 275:1787–1790.
Morrison, E.E., B.N. Wardleworth, J.M. Askham, A.F. Markham, and D.M. Meredith. 1998. EB1, a protein which interacts with the APC tumor suppressor, is associated with the microtubule cytoskeleton throughout the cell cycle. *Oncogene*. 17:3471–3477.
Munemitsu, S., I. Albert, B. Souza, B. Rubinfeld, and P. Polakis. 1995. Regulation of intracellular β-catenin levels by the adenomatous polyposis coli (APC) tumor-suppressor protein. *Proc. Natl. Acad. Sci. USA*. 92:3046–3050.
Munemitsu, S., B. Souza, O. Muller, I. Albert, B. Rubinfeld, and P. Polakis. 1994. The APC gene product associates with microtubules *in vivo* and promotes their assembly *in vitro*. *Cancer Res.* 54:3676–3681.
Nakamura, Y. 1993. The role of the adenomatous polyposis coli (APC) gene in human cancers. *Adv. Cancer Res.* 62:65–87.
Näthke, I.S., C.L. Adams, P. Polakis, J.H. Sellin, and W.J. Nelson. 1996. The adenomatous polyposis coli tumor suppressor protein localizes to plasma membrane sites involved in active cell migration. *J. Cell Biol.* 134:165–179.
Peifer, M. 1995. Cell adhesion and signal transduction: the Armadillo connection. *Trends Cell Biol.* 5:224–229.
Perez, F., G.S. Diamantopoulos, R. Stalder, and T.E. Kreis. 1999. CLIP-170 highlights growing microtubule ends *in vivo*. *Cell*. 96:517–527.
Polakis, P. 1995. Mutations in the APC gene and their implications for protein structure and function. *Curr. Opin. Genet. Dev.* 5:66–71.
Polakis, P. 1997. The adenomatous polyposis coli (APC) tumor suppressor. *Biochim. Biophys. Acta*. 1332:F127–F147.
Pollack, A.L., A.I.M. Barth, Y. Altschuler, W.J. Nelson, and K.E. Mostov. 1997. Dynamics of β-catenin interactions with APC protein regulate epithelial tubulogenesis. *J. Cell Biol.* 137:1651–1662.
Renner, C., J.P. Pfitzenmeier, K. Gerlach, G. Held, S. Ohnesorge, U. Sahin, S. Bauer, and M. Pfreundschuh. 1997. RP1, a new member of the adenomatous polyposis coli-binding EB1-like gene family, is differentially expressed in activated T cells. *J. Immunol.* 159:1276–1283.
Rickard, J.E., and T.E. Kreis. 1990. Identification of a novel nucleotide-sensitive microtubule-binding protein in HeLa cells. *J. Cell Biol.* 110:1623–1633.
Rubinfeld, B., I. Albert, E. Porfiri, C. Fiol, S. Munemitsu, and P. Polakis. 1996. Binding of GSK3β to the APC-β-catenin complex and regulation of complex assembly. *Science*. 272:1023–1026.
Rubinfeld, B., B. Souza, I. Albert, O. Muller, S.H. Chamberlain, F.R. Masiarz, S. Munemitsu, and P. Polakis. 1993. Association of the APC gene product with β-catenin. *Science*. 262:1731–1734.
Sammak, P.J., and G.G. Borisy. 1988. Direct observation of microtubule dynamics in living cells. *Nature*. 332:724–726.
Schulze, E., and M. Kirschner. 1988. New features of microtubule behaviour observed *in vivo*. *Nature*. 334:356–359.
Seeling, J.M., J.R. Miller, R. Gil, R.T. Moon, R. White, and D.M. Virshup. 1999. Regulation of β-catenin signaling by the B56 subunit of protein phosphatase 2A. *Science*. 283:2089–2091.
Shelden, E., and P. Wadsworth. 1993. Observation and quantification of individual microtubule behavior *in vivo*: microtubule dynamics are cell-type specific. *J. Cell Biol.* 120:935–945.
Smith, K.J., D.B. Levy, P. Maupin, T.D. Pollard, B. Vogelstein, and K.W. Kinzler. 1994. Wild-type but not mutant APC associates with the microtubule cytoskeleton. *Cancer Res.* 54:3672–3675.
Su, L.K., K.A. Johnson, K.J. Smith, D.E. Hill, B. Vogelstein, and K.W. Kinzler. 1993a. Association between wild type and mutant APC gene products. *Cancer Res.* 53:2728–2731.
Su, L.K., B. Vogelstein, and K.W. Kinzler. 1993b. Association of the APC tumor suppressor protein with catenins. *Science*. 262:1734–1737.
Su, L.K., M. Burrell, D.E. Hill, J. Gyuris, R. Brent, R. Wiltshire, J. Trent, B. Vogelstein, and K.W. Kinzler. 1995. APC binds to the novel protein EB1. *Cancer Res.* 55:2972–2977.
Tanaka, E., T. Ho, and M.W. Kirschner. 1995. The role of microtubule dynamics in growth cone motility and axonal growth. *J. Cell Biol.* 128:139–155.
Trzepacz, C., A.M. Lowy, J.J. Kordich, and J. Groden. 1997. Phosphorylation of the tumor suppressor adenomatous polyposis coli (APC) by the cyclin-dependent kinase p34. *J. Biol. Chem*. 272:21681–21684.
Vasiliev, J.M. 1991. Polarization of pseudopodial activities: cytoskeletal mechanisms. *J. Cell Sci.* 98:1–4.
Vasquez, R.J., B. Howell, A.M. Yvon, P. Wadsworth, and L. Cassimeris. 1997. Nanomolar concentrations of nocodazole alter microtubule dynamic instability *in vivo* and *in vitro*. *Mol. Biol. Cell.* 8:973–985.
Waterman-Storer, C.M., and E.D. Salmon. 1997. Actomyosin-based retrograde flow of microtubules in the lamella of migrating epithelial cells influences microtubule dynamic instability and turnover and is associated with microtubule breakage and treadmilling. *J. Cell Biol.* 139:417–434.
Wong, M.H., M.L. Hermiston, A.J. Syder, and J.I. Gordon. 1996. Forced expression of the tumor suppressor adenomatosis polyposis coli protein induces disordered cell migration in the intestinal epithelium. *Proc. Natl. Acad. Sci. USA*. 93:9588–9593.